Aerodynamic Characterization of UAV Propellers Using Numerical Analysis and Experimental Testing

Gonçalo Filipe Vizeu
goncalovizeu@tecnico.ulisboa.pt

Instituto Superior Técnico, Universidade de Lisboa, Portugal

December 2023

Abstract

Over the last decades, there have been major developments in Unmanned Aerial Vehicles (UAVs) and, nowadays, they are used for a wide range of commercial applications such as traffic and weather monitoring, deliveries and forest fire detection. This study presents and compares different low-fidelity and high-fidelity aerodynamic numerical models that predict the performance of a UAV propeller for a wide range of flight conditions, such as hovering and vertical climbing. First, the thrust and torque of two commercial propellers are obtained recurring to JavaProp, a software based on the Blade Element Theory. Then, computational fluid dynamics analysis is carried out in the commercial software ANSYS® Fluent®, which includes the construction of the CAD model of the propellers and the flow domain modeling. Furthermore, turbulence model and mesh studies were conducted and the propeller thrust and torque were determined for different flight configurations and flow conditions. Finally, experimental testing to evaluate the aerodynamic performance of one propeller was conducted and the results were validated with computational simulations. The findings of this study suggest that high-fidelity computational models provide results more consistent with experimental testing, whereas the accuracy of results derived from the low-fidelity Blade Element Theory decreases with increasing the propeller angular velocity. Nevertheless, both methods are shown to be suitable for forecasting propeller performance in various flow and flight scenarios.

Keywords: Propeller Design, CFD, Blade Element Theory, Thrust, Torque, Validation

1. Introduction

Unmanned Aerial Vehicles (UAVs) are types of aircraft that can be remotely controlled or fly autonomously by software-controlled flight plans in their embedded systems. The first developments occurred in the mid-1990s and came through the United States Army, as these devices were used for vigilance and survey missions. The use of UAVs for civil and commercial applications came later due to their high costs and the complexity of missions. Due to their exorbitant expenses and intricate assignments, UAVs were once exclusively reserved for military use. Nevertheless, in recent times, UAVs have garnered attention for their diverse commercial applications, such as weather and traffic monitoring and forest fire detection. As battery life improves and flight components such as sensors and processors advance, there has been a relevant growth in the areas where UAVs are employed.

A UAV's primary component is the propeller, which is composed of a series of airfoils connected to form a wing and typically has at least two blades. Propellers are identified by their diameter and pitch, with size measured in inches. For instance, a 14"x13" propeller has a diameter of 14 inches and a pitch of 13 inches. Figure 1 provides a detailed view of these elements, including the hub which attaches the propeller blades to the power source, the leading edge which is the first point of contact with the fluid flow line, and the trailing edge which is the element that ultimately interacts with the fluid flow line. Additionally, the pitch angle β is the angle at which each station of the blade is rotated relative to the propeller disk plane. The diameter of the disk is defined by the rotating propeller, and the chord length, c, is the distance between the leading and trailing edges.

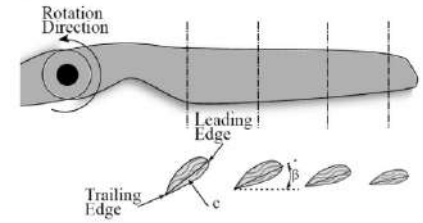

(a) Propeller blade cross sections.

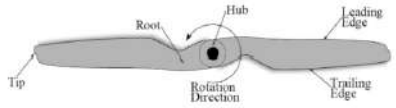

(b) Propeller geometry.

Figure 1: Propeller blade cross sections and geometry. [1]

As a result of the increase in the use of UAVs, there have been numerous advancements made in propeller design for air vehicles. As such, ongoing studies continue to explore the aerodynamic, performance, and structural aspects of propellers. In their experimental study, J. B. Brandt and M. S. Selig [2] made thrust and torque measurements of 79 commercial propellers that are used on small UAVs. The experiments were carried out in a subsonic wind tunnel with a rectangular cross-section of 0.853×1.219 meters and length equal to 2.438 meters at the University of Illinois at Urbana-Champaign (UIUC). The data on the 79 commercial propellers can be found in [3].

Numerical methods have been documented to predict the performance of propellers, primarily in the marine industry, alongside experimental testing. One example is E. Benini's comparison of two analysis methods in [4]. The combined Blade Momentum Element Theory's results were validated against experimental data, and then compared to the results of a 3D CFD analysis conducted in ANSYS® Fluent®. Although both methods were reliable, the CFD analysis was found to be more accurate compared to the first method. A similar analysis comparison was conducted by J. Carroll [5]. Moreover, D. Wilhelm [6] presented an overview of steady-state and unsteady CFD simulations for many rotating flow systems, using OpenFOAM® software. In this paper, a comparison between BEMT and steady-state and unsteady CFD simulations models for a small low-Reynolds propeller is presented.

Other CFD simulations have been reported, but they often focus on hovering scenarios with zero free stream velocity. H. Kutty and P. Rajendran [7] conducted an advancing flow analysis using an unstructured mesh and a moving reference frame to simulate the rotation of the APC 10"x7" Slow Flyer commercial propeller.

2. Propeller Analysis Models

Different numerical methods have been developed in the last century to predict the performance of a rotary-wing propeller. More straightforward approaches like the Blade Element Theory are not so accurate for low values of the Reynolds number. On the other hand, CFD simulations are able to represent suitably the flow field around the propeller and, therefore, to predict its performance. Hence, in this work, these numerical methods can be classified into two groups based on their level of complexity: low-fidelity and high-fidelity.

2.1. Blade Element Theory

The Blade Element Theory was developed by Drzwieck [8] and each blade is divided into sections perpendicular to the radial axis. Figure 2 provides a visual representation of the blade element and the velocities that affect it. At each section, the flow is analyzed as bidimensional and a force balance is applied to determine the lift, drag, thrust, and torque distributions. A final integration over the entire blade gives the performance characteristics of the blade.

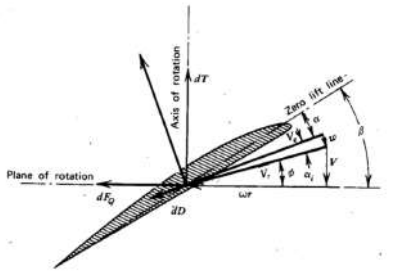

Figure 2: Blade element. [9]

The contribution of each blade element to thrust and torque is given, respectively, by

$$dT = dL\cos(\phi + \alpha_i) - dD\sin(\phi + \alpha_i) \tag{1}$$

and

$$dQ = r[dL\sin(\phi + \alpha_i) + dD\cos(\phi + \alpha_i)], \tag{2}$$

where dL and dD are the section element lift and drag forces, respectively. From bidimensional aerodynamics,

$$dL = \frac{1}{2}\rho V_E^2 c C_l dr \tag{3}$$

$$dD = \frac{1}{2}\rho V_E^2 c C_d dr. \tag{4}$$

The lift coefficient C_l can be found from

$$C_l = \alpha(\beta - \phi - \alpha_i). \tag{5}$$

The thrust, power and torque of a propeller are usually expressed in its coefficient form, respectively

$$C_T = \frac{T}{\rho n^2 D^4} \tag{6}$$

$$C_P = \frac{P}{\rho n^3 D^5} \tag{7}$$

$$C_Q = \frac{Q}{\rho n^2 D^5}, \tag{8}$$

where n is the rotational speed in revolutions per second and D is the propeller diameter.

Finally, J is a quantity called advance ratio and is defined by

$$J = \frac{V}{nD}. \tag{9}$$

2.2. Reynolds-Averaged Navier-Stokes (RANS)

The first problems handled by CFD were relatively straightforward, 2D, incompressible, steady-state situations that usually were limited to laminar flows. It was not until 1967 that the first 3D CFD simulation was completed [10]. Over the years, progress has become much faster as both computational power and modeling approaches advanced.

CFD models employ partial differential equations of conservation of mass and momentum through discrete methods. These equations, known as the Navier-Stokes equations, are formulated as follows for compressible Newtonian flows:

$$\frac{\partial \rho}{\partial t} + \frac{\partial}{\partial x_i}(\rho v_i) = 0 \tag{10}$$

$$\frac{\partial}{\partial t}(\rho v_i) + \frac{\partial}{\partial x_j}(\rho v_j v_i) = -\frac{\partial p}{\partial x_i} + \frac{\partial \tau_{ij}}{\partial x_j} \tag{11}$$

$$\frac{\partial}{\partial t}(\rho E) + \frac{\partial}{\partial x_j}(\rho v_j H) = \frac{\partial}{\partial x_j}(v_i \tau_{ij}) + \frac{\partial}{\partial x_j}\left(k \frac{\partial T}{\partial x_j}\right), \tag{12}$$

where v_i denotes a velocity component $\vec{v} = [v_1, v_2, v_3]^T$ and x_i is a coordinate direction.

A key development was the incorporation of turbulence modeling into the CFD solutions. The concept of "eddy viscosity" was introduced in the first approaches and it reflects an apparent increase in viscosity caused by small-scale chaotic fluid motions. In this study, RANS-based turbulence models, such as k-ϵ and k-ω, are used to investigate the fluid properties around a rotating propeller. The Reynolds-Averaging methodology involves breaking down flow variables into mean and fluctuating components:

$$v_i = \bar{v_i} + v_i' \qquad p_i = \bar{p_i} + p_i'. \tag{13}$$

This means that the Navier-Stokes equations are solved for their mean values.

3. CFD Modelling

Before conducting a high-fidelity numerical analysis of the flow around a rotating propeller, three stages must be completed. The initial stage involves constructing a CAD geometry. Next, a model is built to simulate the flow around the propeller and assign the necessary boundary conditions. The final step involves generating the mesh of the model.

3.1. First stage: Propeller Geometry

In order to build a good representation of the APC 14"x13" Sport and APC 10"x8" Sport propellers, the next procedure was followed:

1. Pictures of the top and front views of the propeller in the study were taken. Both images should be aligned horizontally and have equal diameters.

2. The chord and twist distributions along the blades' radius were obtained from PropellerScanner, a software developed by Martin Hepperly [11]. Several studies have evaluated the accuracy of this software, including Daniel Uhlig's research [12] that compared the values of chord and pitch distributions after slicing a propeller. The results were highly satisfactory, with the chord distributions in agreement and the pitch distributions having only errors between 1° and 2°. PropellerScanner software provides a quick estimate of propeller geometry.

3. The image-processing software ImageJ [13] was used to obtain the coordinates of both the leading and trailing edges of the propellers' blades. Knowing that both analyzed propellers have distributions of Clark-Y airfoils, the distribution of the centers of rotation could be determined.

4. Recurring to Matlab® and SolidWorks®, it was possible to create a precise depiction of the actual propellers, as shown in Figures 3 and 4.

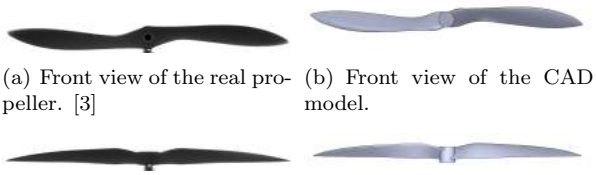

(a) Front view of the real propeller. [3] (b) Front view of the CAD model.

(c) Top view of the real propeller. [3] (d) Top view of the CAD model .

Figure 3: Real vs CAD model APC 14"x13" Sport.

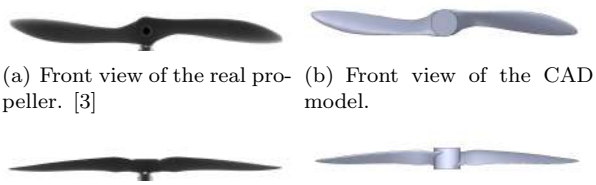

(a) Front view of the real propeller. [3] (b) Front view of the CAD model.

(c) Top view of the real propeller. [3] (d) Top view of the CAD model.

Figure 4: Real vs CAD model APC 10"x8" Sport.

3.2. Second stage: Flow Domain and Boundary Conditions

The second pre-processing stage deals with setting up the CFD environment for analyzing the propeller. The flow domain, shown in Figure 5 comprises two regions - a stationary one that will be solved in a steady reference plane and a rotating one that encloses the propeller and will be solved on a rotating reference frame moving with it. The stationary domain's height and length are eight times the propeller's diameter. Meanwhile, the cylinder diameter of the rotating region is 0,4D, and its height is 1,1D. The choice of geometric boundary for both fluid regions is consistent with previous studies ([7, 14, 15]).

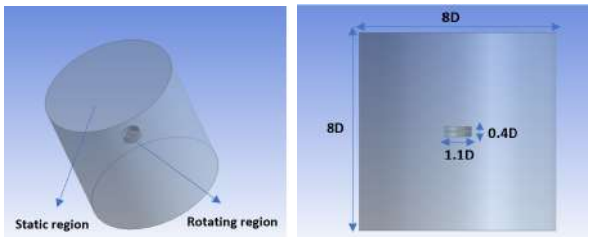

(a) Different fluid regions. (b) Dimensions of the fluid regions.

Figure 5: Flow domain around the rotating propeller.

The APC 14"x13" Sport and APC 10"x8" Sport propellers are designed with two blades, enabling rotational periodicity. As illustrated in Figure 6, only half of the flow domain was calculated, decreasing the number of cells and computational cost.

Before simulating, boundary conditions must be assigned for two types of conditions: hovering flight and vertical climb flight. In hovering flight, only the propeller's rotational speed is set and the free stream velocity is zero. In vertical climb, both the propeller's rotational speed and free stream velocity are set. The boundary conditions assigned for each flight condition are presented in Tables 1 and 2.

Table 1: Boundary conditions for vertical climb flight simulations.

Boundary	Boundary condition	Turbulence boundary condition
Inlet	Velocity-inlet $V = V_{freestream}$	0.1% Turbulence intensity
Outlet	Pressure-outlet $p = p_{atm}$	0.1% Turbulence intensity
Propeller	No-slip wall	-
Periodic outer walls	No-slip wall	-

Table 2: Boundary conditions for hovering flight simulations.

Boundary	Boundary condition	Turbulence boundary condition
Inlet	Pressure-inlet $p = p_{atm}$	0.1% Turbulence intensity
Outlet	Pressure-outlet $p = p_{atm}$	0.1% Turbulence intensity
Propeller	No-slip wall	-
Periodic outer walls	No-slip wall	-

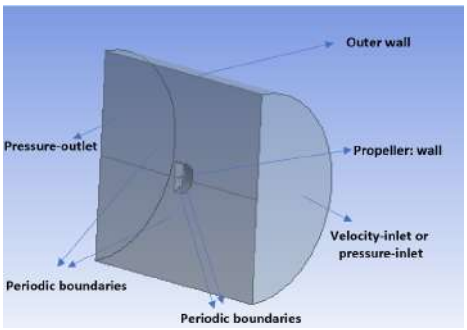

Figure 6: Boundary conditions.

3.3. Third stage: Mesh Generation

In order to effectively simulate and predict performance, it is imperative to acquire a mesh of the domain that meets high standards of quality. This will yield dependable results that closely resemble those generated by experimental testing within a wind tunnel. The quality of the mesh is a determining factor in the rate of convergence, simulation duration, and overall performance.

ANSYS® Meshing™ was used to generate the mesh. For the present investigation, a non-structured mesh comprising tetrahedral elements was opted for both the stationary and rotating fluid domains. Prism elements were used for crafting the boundary layer encircling the propeller walls. By leveraging an unstructured mesh, the complex geometry mandated minimal intervention from the user. Figure 7 provides a closer view of the unstructured mesh generated in both fluid regions.

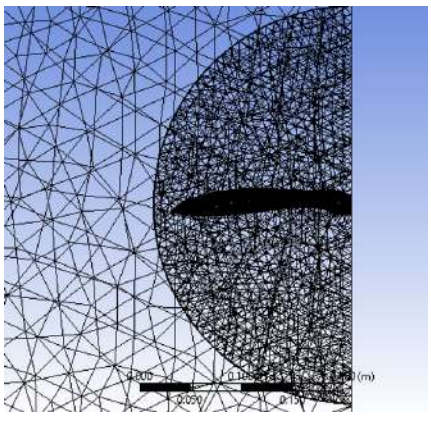

Figure 7: Mesh generation.

For the boundary layer enveloping the propeller walls, prism elements were employed. Figure 8 shows the boundary layer mesh at 75% of the blade radius.

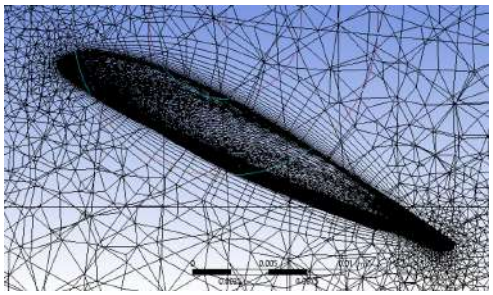

Figure 8: Boundary layer mesh at 75% of the blade radius.

4. Simulated Propeller Performance

The performance results of the APC 14"x13" Sport and APC 10"x8" Sport commercial propellers were obtained through a low-fidelity numerical analysis based on the Blade Element Theory and through a high-fidelity numerical analysis carried out in ANSYS® Fluent®. Moreover, these results were compared with the experimental testing conducted at UIUC, [3].

4.1. Low-Fidelity vs High-Fidelity Analyses

The performance results based on the Blade Element Theory were obtained using JavaProp software. JavaProp [16] is a tool used for the design and analysis of propellers and wind turbines. The implemented classical blade element design and analysis methods are based on coupling momentum considerations with 2D airfoil characteristics. It is, therefore, possible to consider different airfoil sections and the impact of their characteristics on the rotor performance.

4.2. Propeller 1: APC 14"x13" Sport

As previously mentioned, this propeller boasts a 14-inch diameter and 13-inch pitch. To conduct a successful CFD analysis, it is essential to have a thorough understanding of the system's physics and a detailed description of its geometry. In order to build the model that represents the best flow conditions and to obtain the most accurate possible results regarding each propeller's performance, some studies on the mesh, turbulence model and rotating region were made.

4.2.1. Mesh Refinement Analysis

A mesh independence study for the APC 14"x13" propeller was carried out for the following conditions:

- Propeller angular velocity: $\Omega = 3003$ RPM;
- Advanced ratio: $J = 0,581$.

The solutions of the thrust and torque were obtained for eight different cell element sizes and are illustrated in Figure 9.

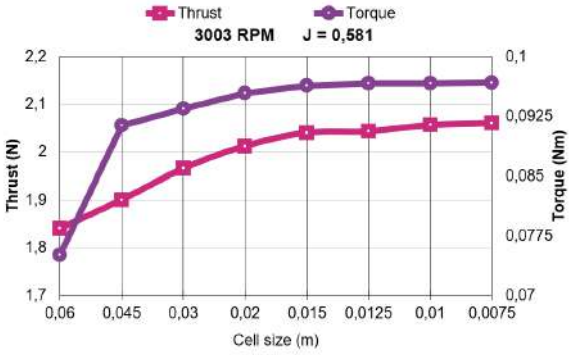

Figure 9: Mesh refinement. APC 14"x13" Sport.

Based on the data presented, it is clear that implementing mesh refinement enhances the solution. Interestingly, the number of mesh cells does not seem to have any significant impact on the outcome as long as the element size is lower than 0.015 meters. Consequently, to ensure optimal outcomes while minimizing solution time, a thorough performance analysis was carried out using a model featuring a mesh element size equal to 0.01 meters.

4.2.2. Turbulence Model Analysis

The turbulence model study for the APC 14"x13" propeller was carried out for a rotational velocity of 2998 RPM. Table 3 presents the results obtained for Standard $k-\epsilon$ and SST $k-\omega$ models.

Table 3: Turbulence model study. APC 14"x13" Sport.

2998 RPM	k-ε standard model		k-ω SST model	
J	(%) ε_{ct}	(%) ε_{cq}	(%) ε_{ct}	(%) ε_{cq}
0,206	1,07	3,91	-5,79	3,85
0,31	-2,74	6,32	-9,04	-1,37
0,381	-3,79	4,59	-8,37	-5,87
0,412	-3,83	3,47	-7,94	-6,36
0,485	-4,19	2,26	-8,40	-8,14
0,277	-1,59	5,84	-8,28	0,36
0,553	-0,68	1,41	-8,16	-8,72
0,617	1,25	1,76	-6,72	-8,36

It can be seen that both models have a tendency to underpredict the thrust when compared to experimental results. However, the Standard $k-\epsilon$ model tends to overpredict the torque, whereas the SST $k-\omega$ model tends to underpredict it. In conclusion, both models accurately depict the flow conditions around the rotating propeller. However, the Standard $k-\epsilon$ model produces more accurate results. Therefore, the remaining performance analyses will be conducted using the Standard $k-\epsilon$ turbulence model.

4.2.3. Performance at 2003 RPM

Vertical climb flight simulations were carried out using a mesh with around 3 200 000 cells and using the Standard $k-\epsilon$ turbulence model.

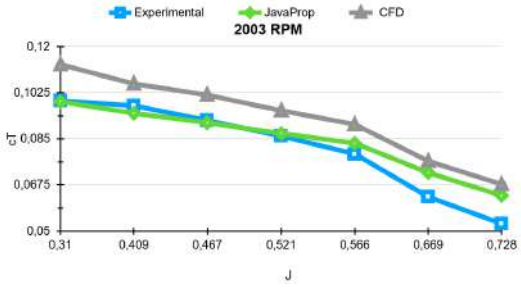

(a) Thrust coefficient.

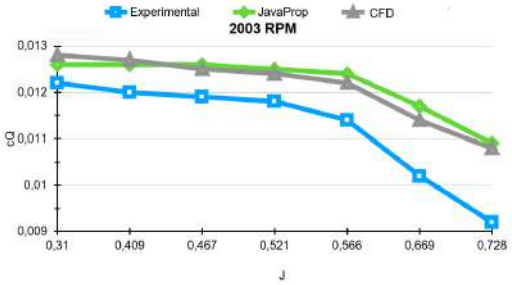

(b) Torque coefficient.

Figure 10: Performance. Ω = 2003 RPM. APC 14"x13" Sport.

In Figure 10, a comparison is shown between the results obtained from using JavaProp, ANSYS® Fluent® and experimental testing. The RANS-based approach resulted in an overestimation of both thrust and torque, with an average error of 15,5% for the thrust coefficient and 7,89% for the torque coefficient. In contrast, the results from JavaProp, which uses Blade Element Theory, were found to be more accurate, with an average error of only 5,29% for the thrust coefficient and 8,65% for the torque coefficient when compared to experimental data.

4.2.4. Performance at 2508 RPM

Figure 11 shows the comparisons of the results obtained through JavaProp and ANSYS® Fluent® and the experimental testing for a rotational propeller velocity of 2508 RPM.

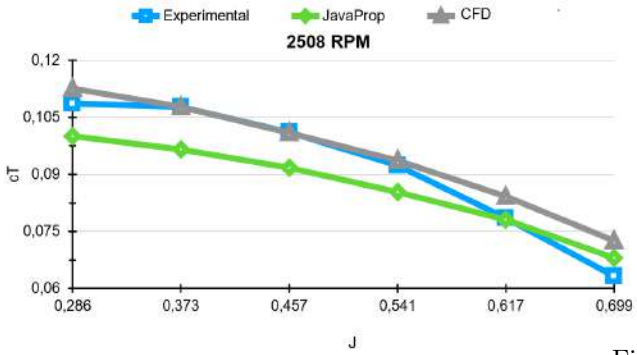

(a) Thrust coefficient.

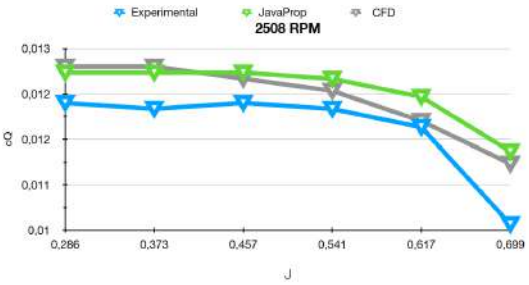

(b) Torque coefficient.

Figure 11: Performance. Ω = 2508 RPM. APC 14"x13" Sport.

The high-fidelity analysis provided more accurate results when compared to the low-fidelity. In the first mentioned method, the maximum error was 14,66% for the thrust coefficient and 9,91% for the torque coefficient at an advanced ratio of 0,699. Compared to the results at a rotational speed of 2003 RPM, the solution now provides a more accurate representation of the actual flow. The low-fidelity analysis continued to provide accurate results; the highest deviation is -10,48% for the thrust coefficient and 11,71% for the torque coefficient. Furthermore, both analyses display a sudden increase in error when the free stream velocity and advance ratio reach their peak points.

4.2.5. Performance at 2998 RPM

Figure 12 shows the comparisons of the results obtained through JavaProp and ANSYS® Fluent® and the experimental testing for a rotational propeller velocity equal to 2998 RPM.

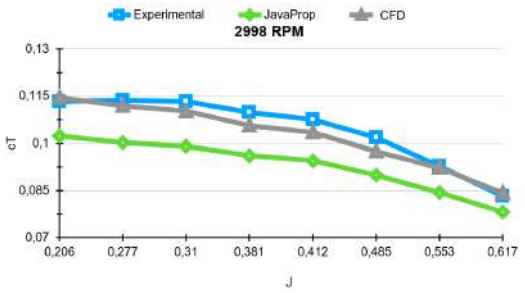

(a) Thrust coefficient.

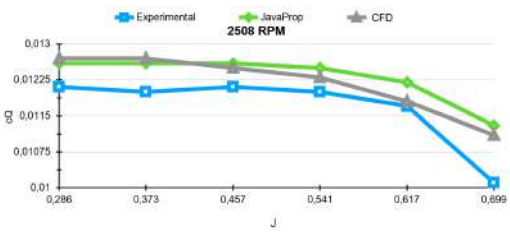

(b) Torque coefficient.

Figure 12: Performance. Ω = 2998 RPM. APC 14"x13" Sport.

It can be seen that ANSYS® Fluent® accurately predicted the flow properties of the rotating propeller for the referred conditions, with the thrust and torque coefficients showing results similar to those obtained through experimental testing. The maximum level of inconsistency was -4,19% for the thrust coefficient and 6,3% for the torque coefficient. In contrast, the low-fidelity analysis significantly underestimated the thrust and overestimated the torque, with an average error of -10,70% for the thrust coefficient and 4,46% for the torque coefficient.

4.2.6. Performance at 3508 RPM

Figure 13 shows the comparisons of the results obtained through JavaProp and ANSYS® Fluent® and the experimental testing for a rotational propeller velocity of 3508 RPM.

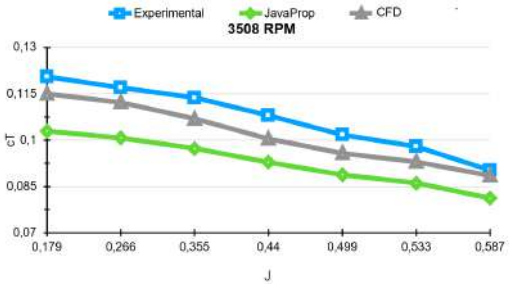

(a) Thrust coefficient.

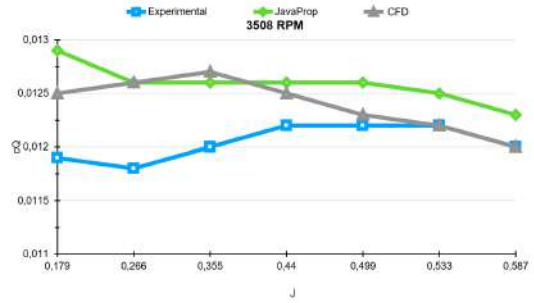

(b) Torque coefficient.

Figure 13: Performance. Ω = 3508 RPM. APC 14"x13" Sport.

Based on the presented data, the high-fidelity analysis solution underestimated the thrust and overestimated the torque. In fact, the maximum error for the thrust coefficient was -7,04%, while the torque coefficient has a maximum error of 7,13%. However, it's worth noting that the accuracy of the torque results improved as the advance ratio increased. Alternatively, the results from JavaProp software demonstrated a significant underestimation of thrust and an overestimation of torque. The thrust coefficient had a maximum inconsistency of -14,44%, while the torque coefficient had a maximum inconsistency of 7,84%. Nevertheless, as with the high-fidelity analysis solution, the accuracy of both thrust and torque solutions improved with higher advance ratios.

Analyzing the overall performance of the APC 14"x13" Sport propeller, it becomes apparent that the accuracy of CFD simulations is consistently high, with the exception of instances when the rotational velocity is at its lowest. In such cases, the accuracy of the simulations experiences a notable decrease. In contrast, as the rotational velocity of the propeller increases, Blade Element Theory is proven to be less accurate. This is due to flow disruptions that cannot be predicted by the theory, caused by an increase in the Reynolds number of the flow around the propeller.

4.3. Propeller 2: APC 10"x8" Sport

The second propeller analyzed is characterized by a 10-inch diameter and 8-inch pitch. Similar studies to the ones conducted with the APC 14"x13" Sport model were also conducted for the APC 10"x8" Sport propeller.

4.3.1. Mesh Refinement Analysis

Instead of analyzing the convergence of the torque and thrust, an analysis of the accuracy of these parameters was carried out. Hence, three different meshes, summarized in Table 4, were generated and investigated.

Table 4: Mesh refinement study. APC 10"x8" Sport.

Mesh	Cell element size (m)	Number of cells
Coarse	0,055	629 411
Standard	0,04	1 085 187
Fine	0,0275	1 994 231

The thrust and torque coefficients obtained are summarized in Table 5.

Table 5: Mesh refinement results. APC 10"x8" Sport.

Mesh	C_T	$(\%)\epsilon_{ct}$	C_Q	$(\%)\epsilon_{cq}$
Coarse	0,1054	-3,24	0,01235	10,89
Standard	0,1080	-0,85	0,01170	4,98
Fine	0,1091	0,17	0,01097	-1,57

It is evident that the finer grid yields the most precise outcomes in comparison to the experimental testing. Thus, to evaluate the performance of the APC 10"x8" Sport propeller, the simulations were carried out using a model with a mesh element size equal to 0,0275 meters.

4.3.2. Turbulence Model Analysis

The turbulence study for the APC 10"x8" propeller was carried out for a rotational propeller velocity

equal to 3900 RPM. Table 6 presents the results obtained for the different turbulence models.

Table 6: Turbulence model study. APC 10"x8" Sport.

Turbulence model	C_T	$(\%)\epsilon_{ct}$	C_Q	$(\%)\epsilon_{cq}$
Standard $k-\epsilon$	0,1176	8,01	0,0111	-0,56
Realizable $k-\epsilon$	0,1240	13,90	0,0105	-5,81
SST $k-\omega$	0,1091	0,17	0,01097	-1,57
Standard $k-\omega$	0,1030	-5,46	0,0125	11,87

The predictions made by both $k-\epsilon$ models regarding the thrust are higher than the experimental testing, with the Realizable model having an error over 10%. On the other hand, the Standard $k-\omega$ model overestimates the torque. The SST $k-\omega$ model provides the most accurate results, making it the preferred option for the remaining simulations and a precise representation of the real flow conditions.

It should be noted that the APC 14"x13" Sport propeller's turbulence model with the best results was the Standard $k-\epsilon$. This highlights the fact that there is no universal turbulence model as each model has its own advantages and disadvantages, and the accuracy of the model depends on the flow conditions.

4.3.3. Performance at Hovering Conditions

Hovering flight simulations (J=0, i.e., free stream velocity equal to zero) were carried out using a mesh of around 2 million cells and using the SST $k-\omega$ turbulence model.

Figure 14 shows the results for thrust and torque, respectively, obtained through JavaProp, ANSYS® Fluent® and the experimental testing ([3]) when J=0.

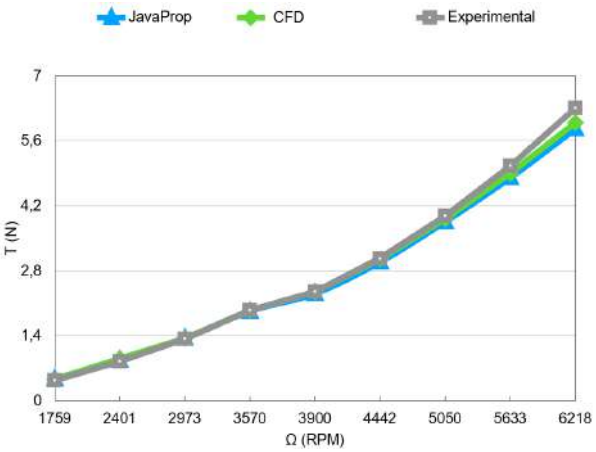

(a) Thrust.

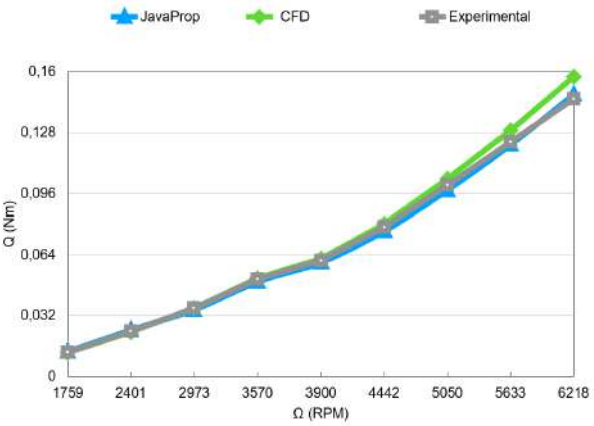

(b) Torque.

Figure 14: Performance. APC 10"x8" Sport.

Based on the CFD simulations' results, the maximum error observed was -4,89% for the thrust coefficient and -2,84% for the torque coefficient. On average, the error was found to be 0,22% for the thrust coefficient and -0,84% for the torque coefficient. For low angular velocities, the thrust and torque are overpredicted. Once the angular velocity of the propeller is increased, it is possible to visualize a tendency to underpredict both thrust and torque. Overall, the analysis has demonstrated its ability to accurately predict flow properties across all configurations. In contrast, when using low-fidelity numerical analysis, the maximum error for the thrust coefficient is -7,12% and for the torque coefficient it is 7,80%. Additionally, the average error for the thrust coefficient is -1,29% and for the torque coefficient it is 2,02%. While the accuracy of these results is not as high as those obtained with ANSYS® Fluent®, the Blade Element Theory is still an effective method for predicting the performance of a rotating propeller.

5. Experimental Testing and Validation

5.1. Experimental Setup

This Section addresses the experimental aerodynamic performance measurements of the APC 10" × 8" Sport propeller conducted using a force balance, shown in Figure 15, as designed and employed in a study authored by M. Borges [17]. The experimental testing was carried out at Instituto Superior Técnico. To obtain the required data on the propeller's performance, the structure was equipped with a load cell, voltage and current sensors, and a RPM sensor.

Additionally, an Electronic Speed Control (ESC) was implemented to regulate and manage the motor's velocity. This device enables speed control through a PMW signal (Pulse Width Modulation). The control process was executed using the

Figure 15: Force balance at Instituto Superior Técnico.

LabView® Interface software.

5.2. Static Tests

As explained earlier, propeller performance analysis involves evaluating two configurations: static and dynamic conditions. Static conditions refer to situations where there is no income flow on the propeller. In this study, only static tests were conducted. Hence, the propeller APC 10" × 8" Sport was mounted in combination with a brushless motor replicating hovering flight conditions.

The throttle of the motor level ranged from 15% and 60% in small increments (5 to 10 seconds at each level), leading to some uncertainty. In the experimental tests, different parameters were analyzed:

- Thrust;
- Electrical power.

In Figure 16, it is possible to visualize the graphics with the data acquired on the experiments changing the throttle of the motor level (associated with the change in angular velocity).

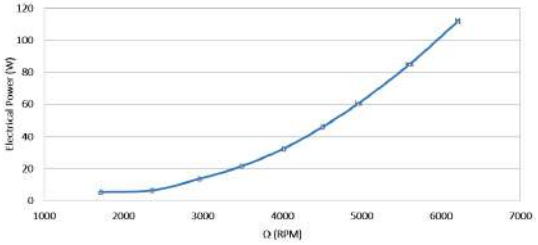

(a) Electrical Power.

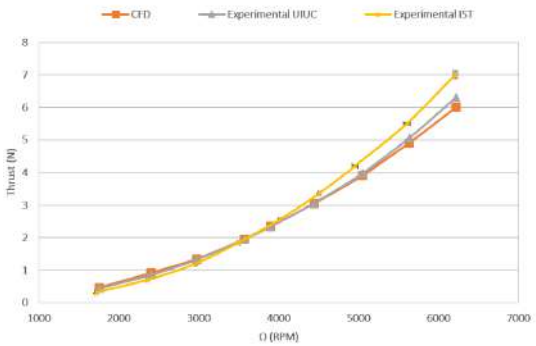

(b) Thrust.

Figure 16: Experimental performance. APC 10"x8" Sport.

As motor power and propeller speed are increased, the precision and accuracy of data collected at IST may decrease due to calibration challenges and environmental conditions. Factors such as temperature and pressure can significantly impact the recorded data, potentially causing inconsistencies in the values obtained. However, despite these difficulties, the experimental data collected at IST remains valuable and can be validated as it demonstrates similar trends to results obtained from UIUC testing and CFD simulations.

6. Conclusions

This study delves into the various techniques utilized for predicting the aerodynamic performance of a drone propeller. These methods can be classified into two groups based on their level of complexity: low-fidelity and high-fidelity numerical analyses.

The study involved two commercial propellers, the APC 14"x13" Sport and APC 10"x8" Sport, under a variety of flight configurations, such as hovering and vertical climb. To obtain thrust and torque, ANSYS® Fluent® and JavaProp software were employed. To ensure the accuracy of the findings, the thrust and torque measurements were compared to the experimental testing conducted at the University of Illinois Urbana-Champaign [3].

A comprehensive computational study was conducted to determine the optimal turbulence model for analyzing propeller performance. The $k-\epsilon$ Standard model was found to provide more accurate results for the APC 14"x13" Sport propeller, while the $k-\omega$ SST model was more effective for the APC 10"x8" Sport propeller. Selecting the most appropriate model depends on the specific flight conditions being analyzed.

Vertical climb flight simulations were performed for APC 14"x13" Sport propeller at different rotational and free stream velocities. Based on observations, the CFD simulations yielded consistently

accurate results for all flight configurations, except when the rotational propeller velocity decreased, resulting in significant errors. Using the Blade Element Theory in JavaProp software led to the conclusion that the accuracy decreases as the propeller angular velocity increases. Hovering flight (no incoming free stream) simulations were conducted for the APC 10"x8" Sport propeller at different rotational velocities ranging from 1759 RPM to 6218 RPM. The CFD simulations showed a maximum discrepancy of -4,89% for the thrust coefficient and -2,84% for the torque coefficient. Meanwhile, the Blade Element Theory approach had a maximum error of -7,12% for thrust and 7,80% for torque.

A series of static experimental tests were conducted using a force balance built and calibrated at Instituto Superior Técnico. The tests aimed to evaluate the performance of the APC 10"x8" Sport propeller. The testing results showed a high correlation between the CFD simulations and the experiments carried out at the University of Illinois at Urbana-Champaign (UIUC).

Based on the results obtained, both the low-fidelity and high-fidelity methods have demonstrated a reliable ability to forecast propeller efficiency in various flow and flight scenarios. These findings suggest that either method may be suitable for use in various applications requiring accurate propeller efficiency predictions.

References

[1] E. V. Loureiro, N. L. Oliveira, P. H. Hallak, F. S. Bastos, L. M. Rocha, and A. C. C. L. R. G. P. Delmonte, "Evaluation of Low Fidelity and CFD Methods for the Aerodynamic Performance of a Small Propeller," *Aerospace Science and Technology, Volume 108*, 2021.

[2] J. B. Brandt and M. S. Selig, "Propeller Performance Data at Low Reynolds Numbers," *49th AIAA Aerospace Science Meetings, Orlando, USA*, 2011. DOI: 10.2514/6.2011-1255

[3] J. B. Brandt, R. W. Deters, G. K. Ananda, and M. S. Selig. UIUC Propeller Database. https://m-selig.ae.illinois.edu/props/propDB.html/. (accessed: March 2023).

[4] E. Benini, "Significance of Blade Element Theory in Performance Prediction of Marine Propellers," *Ocean Engineering*, vol. 31, pp. 957–974, 06 2004. DOI: 10.1016/j.oceaneng.2003.12.001

[5] J. Carroll and D. Marcum, "Comparison of a Blade Element Momentum Model to 3D CFD Simulations for Small Scale Propellers," *SAE International Journal of Aerospace*, vol. 6, pp. 721–726, 07 2013. DOI: 10.4271/2013-01-2270

[6] D. Wilhelm, "Rotating Flow Simulations with OpenFOAM," *International Journal of Aeronautical Science & Aerospace Research*, vol. 1, no. 001, 2015.

[7] H. Kutty and P. Rajendran, "3D CFD Simulation and Experimental Validation of Small APC Slow Flyer Propeller Blade," *Aerospace*, vol. 4, no. 1, 2017. DOI: 10.3390/aerospace4010010

[8] S. Drzewiecki, *Théorie générale de l'hélice: hélices aériennes et hélices marines*. Gauthier-Villars et cie., 1920.

[9] B. W. McCormick, *Aerodynamics, Aeronautics and Flight Mechanics*. John Wiley and Sons, 2nd Edition, 1994, ISBN-13: 978-0471575061.

[10] J. Gorman, S. Bhattacharyya, L. Cheng, and J. P. Abraham, *Applications of Computational Fluid Dynamics Simulation and Modeling*. S. Bhattacharyya, 2022, ISBN-13: 978-1839682476, ch. 2. Turbulence Models Commonly Used in CFD.

[11] M. Hepperly. PropellerScanner. http://mh-aerotools.de. (accessed: March 2023).

[12] D. V. Uhlig, ""Post Stall Propeller Behavior at Low Reynolds Numbers"," Master's thesis, University of Illinois at Urbana-Champaign, USA, 2007.

[13] C. A. Schneider, W. S. Rasband, and K. W. Eliceiri, "NIH Image to ImageJ: 25 Years of Image Analysis. Nature Methods," *Nature Methods*, vol. 9, no. 7, pp. 671–675, 2012.

[14] A. Ghenaiet and A. Halimi, "Aerodynamic Characterization of a High Speed Propeller," in *Turbo Expo: Power for Land, Sea, and Air*, vol. 45578. American Society of Mechanical Engineers, 2014.

[15] M. Stajuda, M. Karczewski, D. Obidowski, and K. Jóźwik, "Development of a CFD model for Propeller Simulation," *Mechanics and Mechanical Engineering*, vol. 20, 2016.

[16] M. Hepperly. JavaProp. http://www.mh-aerotools.de/airfoils/javaprop.htm. (accessed: March 2023).

[17] M. Borges, "Design of an Apparatus for Wind Tunnel Tests of Electric UAV Propulsion Systems," Master's thesis, Instituto Superior Técnico, Portugal, 2015.